Sensor placement in nuclear reactors based on the generalized empirical interpolation method

J P Argaud, B P Bouriquet, Helin Gong, Yvon Maday, Olga Mula

Sensor placement in nuclear reactors

J.P. Argaud[a], B. Bouriquet[a], H. Gong[a,b], Y. Maday[b,c,d], O. Mula[e]

[a] *Électricité de France, R&D, 7 boulevard Gaspard Monge, 91120 Palaiseau, France.*
[b] *Sorbonne Universités, UPMC Univ Paris 06 and CNRS UMR 7598, Laboratoire Jacques-Louis Lions, F-75005, Paris, France.*
[c] *Institut Universitaire de France.*
[d] *Division of Applied Mathematics, Brown University, Providence RI, USA.*
[e] *Université Paris-Dauphine, PSL Research University, CNRS, UMR 7534, CEREMADE, 75016 Paris, France.*

Abstract

In this paper, we apply the so-called generalized empirical interpolation method (GEIM) to address the problem of sensor placement in nuclear reactors. This task is challenging due to the accumulation of a number of difficulties like the complexity of the underlying physics and the constraints in the admissible sensor locations and their number. As a result, the placement, still today, strongly relies on the know-how and experience of engineers from different areas of expertise. The present methodology contributes to making this process become more *systematic* and, in turn, simplify and accelerate the procedure.

Keywords: generalized empirical interpolation method, sensor placement, data assimilation, nuclear safety
PACS: 02.30.Jr, 02.30.Mv, 02.60.Cb, 02.60.Ed, 02.60.Gf
2010 MSC: 65D05, 41A29, 65Z05, 65N99, 93B15

1. Introduction

Energy production based on nuclear reactions are probably among the most demanding source of energy with respect to safety standards. Tight criteria have to be satisfied both at design and operation levels. What is essentially required in all cases is the accurate knowledge of significant quantities like temperature, neutron flux, power, irradiation or fluence. The quantities can be global outputs like the maximum or average temperature or the total generated power but the knowledge of more detailed information like temperature, flux and/or power maps in the whole reactor may also be required. Regardless of the exact quantity of interest, the knowledge of these quantities is accessed either through the study of parametrized models and/or through measurement data collected from the reactor itself. Once a suitable model has been found, it is sometimes confronted to data coming from real experiments. The data can, in turn, be useful to correct the model. Once a model and/or sensor measurements are given, the goal is usually to reconstruct as precisely as possible the quantity of interest in order to retrieve more safety, power efficiency or any other significant criterion.

- At design stages, the procedure consists, in very general lines, in looking for the parameters of the model which lead to the safest configuration of the core for a given energy production.

- At the operation level, the information is primarily obtained via sensor measurements. Their placement has to be carefully optimized in order to retrieve as much information as possible while the reactor is running. In any of these optimization contexts, the experience of the engineers plays a crucial role in order to find acceptable configurations. What is more, due to the complexity of the physics, it is even sometimes necessary to combine the expertise of engineers from different fields and the optimization process could require several iterations between experts before satisfying all the desired criteria.

In this context, this paper is a contribution to making these tasks become more *systematic*. For this, we present a novel methodology from the fields of data assimilation and reduced basis to the field of reactor simulations. The main idea is to approximate the quantity of interest (say, the neutron flux) with a linear combination of a few well chosen terms. It is well known that the neutron flux can be accurately represented as the solution of a (parameter dependent) transport/diffusion equation. The above "well chosen terms" are then particular solutions to the model problem (obtained by appropriate selection of the parameters), this is the reduced basis part. The "data assimilation" part is obtained by the Generalized Empirical Interpolation Method (GEIM, see [1, 2]) where the above linear combination is defined in such a way that the measures on the data coincide with the data coming out from the core.

The construction combines the knowledge of a physical model that describes the underlying physics with data measured in the reactor itself. A feature of this methodology which might be of interest to the community in terms of accuracy and rapidity is that the information from the model and the measurements is incorporated *simultaneously* and not in a sequential manner as the classical procedures in nuclear engineering usually require.

We would like to emphasize that GEIM belongs to a broader class of recovery methods which gathers other approaches like the PBDW methodology of [3] where the use of data allows, not only to reconstruct the quantities of interest, but also to correct the possible bias in the mathematical model. Here we shall not use this feature and assume that the mathematical model is perfect. The whole class is subject of current active research in the community of applied mathematics (see, e.g., [4, 5, 6, 7]) since it carries potential to address in a unified methodology different types of inverse or uncertainty quantification problems arising in a large variety of physical systems. Among the possible applications of the method to the field of reactor physics stand (i) the search for optimal sensor locations to measure certain quantities of interest during the operation of the core, (ii) the acceleration in the search for optimally safe and/or efficient core configurations since GEIM is a real time reconstruction of the quantities of interest. Much more ambitious is the possibility to take into account the accuracy of the sensors. Indeed one could be interested in using few, very accurate, sensors and more, less accurate ones. The natural questions are then to place them

in an optimal way. Another related question is : given a certain budget, what is the best location/quality/number of sensors to recover the best approximation. We shall consider these questions in a latter contribution.

At any rate, we emphasize that the method cannot completely replace the experience of experts of the field. It should be seen as a tool to assist them in doing these tasks more efficiently and specially in a more *systematic* way.

Since the number of potential applications is relatively broad, in this paper we restrict ourselves to idea (i). For this, we start in section 2 by an explanation of GEIM. In section 3, we implement GEIM to a nuclear reactor physical model. Then, in section 4, we present a numerical example illustrating the search for appropriate sensor locations to reconstruct flux and power maps in a nuclear reactor. In this respect, the present paper is a follow up of the numerical results announced in [8]. The presentation of GEIM in section 2 is deliberately oriented towards explaining how to implement it in the context of neutronics. This is done by taking the neutron flux and the power as examples of quantities of interest. We hope that readers with other fields of interest will be able to extrapolate the idea to their own problems. Also, the interested reader can refer to [2, 7] for the theoretical foundations and a more general presentation. We finish the article by briefly explaining generalizations of GEIM, current theoretical challenges and new perspectives regarding nuclear physics applications (see section 5).

2. The Generalized Empirical Interpolation Method

2.1. Preliminaries

By way of preliminaries, we introduce the mathematical notations used throughout this paper. Let $\mathcal{X}$ be a Banach space defined over a domain physical $\mathcal{R} \subset \mathbb{R}^d$ ($d \geq 1$) and let $\|\cdot\|$ be the associated norm. In our case $\mathcal{R}$ will be the reactor domain and $\mathcal{X}$ will be either $L^2(\mathcal{R})$, $H^1(\mathcal{R})$ or $L^\infty(\mathcal{R})$ or product of these spaces, e.g. $H^1(\mathcal{R})^2 \times L^\infty(\mathcal{R})$.

2.2. Idea of the Generalized Empirical Interpolation Method

In order to understand a physical phenomena/state of interest, we can access either through an *implicit* way based on the knowledge of a physical model or through an *explicit* way based on the knowledge from measurement data collected from the physical system itself.

i) Knowledge from physical model implicitly. In general, the physical model can be described as implicit form

$$\mathcal{F}(f, \mu) = 0, \tag{2.1}$$

e.g., a partial differential equation (PDE), where f is a representation of the state, which depends on $p \geq 1$ essential parameters gathered in a vector $\mu \in \mathbb{R}^p$. To account for different possible working conditions for the particular physical phenomena, we assume that these p parameters vary in some range $\mathcal{D} \subset \mathbb{R}^p$, by solving this implicit

form numerically for each μ, we get a set of all possible states (e.g., neutron flux or power) given by

$$\mathcal{M}_f \coloneqq \{f(\cdot,\mu) \ : \mu \in \mathcal{D}\}, \tag{2.2}$$

which is called the manifold of states. Reduced basis method theory [7, 9**? ?**] points out that, exploiting the knowledge of the set $\mathcal{M}_f$ of all quantities of interest when the parameters vary, for a particular μ the corresponding state $f(\cdot,\mu)$ in $\mathcal{M}_f$ may be well approximated by function in a small dimensional (generally unknown) space [1].

ii) Knowledge from measurement data explicitly. The physical state of interest can also be represented explicitly as $f(x,\mu)$ at point x for a particular parameter state μ by point-wise sensors that are installed in $\mathcal{R}$, or less explicitly represented on average, e.g., a local average over f centered at $x \in \mathcal{R}$. Let us assume that we have a dictionary of linear functionals $\sigma \in \Sigma$, assumed to be continuous in some sense, e.g. in $L^2(\mathcal{R})$. With no loss of generality, the representation of different sensors can be denoted as

$$\sigma(f,x), \tag{2.3}$$

the measurement of f at a position $x \in \mathcal{R}$ by a certain sensor.

Besides, there is possibility to represent the physical state of interest based on the knowledge from physical model combining with measurement. In very practical terms, GEIM can be seen as a method to approximate all the possible states (given by $\mathcal{M}_f$) by a well chosen element of a suitable n-dimensional subspace $X_n \subset \mathcal{X}$ with small dimension (reduced model). The approximation is done via interpolation from measured data. GEIM allows to construct both the n-dimensional subspace X_n and the specification (position) of the data acquisition, in a recursive way. Like most model reduction methods, GEIM exploits the knowledge of the set $\mathcal{M}_f$ of all quantities of interest when the parameters vary and the fact that $\mathcal{M}_f$ may be well approximated by a small dimensional (generally unknown) space. This could be approached based on the following two hypothesis (and facts): i) *unisolvence property* for sensors, say, if $f \in \mathcal{X}$ is such that $\sigma(f) = 0, \forall \sigma \in \Sigma$, then $f = 0$; ii) $\mathcal{M}_f$ *with small Kolmogorov n-width*. Based on GEIM, we first

- select a set of functions $\{f(\cdot,\mu_1),\cdots,f(\cdot,\mu_n)\}$ from the manifold $\mathcal{M}_f$ and the associated basis functions $(q_1,\ldots,q_n)$ that span a n-dimensional space $X_n = \text{span}\{q_1,\ldots,q_n\}$ or equivalently $X_n = \text{span}\{f(\cdot,\mu_1),\cdots,f(\cdot,\mu_n)\}$,
- and a set of locations $x_1,\ldots,x_n \in \mathcal{R}$ of the sensors,

with a greedy algorithm. Then, any function $f(\cdot,\mu) \in \mathcal{M}_f$ can be approximated with a function $\mathcal{J}_n[f](\mu) \in X_n$ defined as

$$\mathcal{J}_n[f](\mu) \coloneqq \sum_{j=1}^{n} c_j(\mu) q_j. \tag{2.4}$$

[1] From a mathematical point of view this means that $\mathcal{M}$ has a small Kolmogorov n-width (we refer to [9] for reasons why $\mathcal{M}_f$ may be with small Kolmogorov n-width).

The $c_j(\mu)$ are coefficients which depend on the parameters μ. They are computed using measurement information by imposing the interpolating conditions

$$\sigma\left(f(\cdot,\mu),x_k\right)=\sigma\left(\mathcal{J}_n[f](\mu),x_k\right),\ k\in\{1,\dots,n\},\tag{2.5}$$

where we see that, the coefficients $(c_1,\dots,c_n)$ are the solution of a $n\times n$ linear system of equations. Most of the times, the reconstruction gives enough accuracy for a small dimension n of X_n. We refer to [2, 7] for the mathematical analysis of the approach.

Note that when solving the manifold $\mathcal{M}_f$, we assume that the mathematical model is perfect, other approaches like the PBDW methodology of [3] where the use of data allows, not only to reconstruct the quantities of interest, but also to correct the possible bias in the mathematical model.

2.3. GEIM greedy algorithm

Based on the sensors' *unisolvence property* hypothesis and $\mathcal{M}_f$ of small Kolmogorov n-width hypothesis, we start by finding the parameter μ_1 in $\mathcal{M}_f$ such that

$$\|f(\cdot,\mu_1)\|=\max_{\mu\in\mathcal{D}}\|f(\cdot,\mu)\|.\tag{2.6}$$

The state $f(\cdot,\mu_1)$ defines $X_1^{(f)}=\text{span}\{f(\cdot,\mu_1)\}$. The first sensor location x_1 is the one such that

$$|\sigma\left(f(\cdot,\mu_1),x_1\right)|=\max_{x\in\mathcal{R}}|\sigma\left(f(\cdot,\mu_1),x\right)|.\tag{2.7}$$

To facilitate the practical computation of the generalized interpolant, we do a change of basis in X_1. Instead of working with $f(\cdot,\mu_1)$ as basis function, we use

$$q_1=\frac{f(\cdot,\mu_1)}{\sigma(f(\cdot,\mu_1),x_1)}.$$

For any $\mu\in\mathcal{D}$, the generalized interpolant of $f(\cdot,\mu)$ is

$$\mathcal{J}_1[f](\mu)=c_1(\mu)q_1\tag{2.8}$$

and $c_1(\mu)$ is found with the interpolating conditions (2.5) for $n=1$. We then proceed by induction. Assume that, for a given $M\geq 1$, we have selected a set of states $\{f(\cdot,\mu_j)\}_{j=1}^M$ and the associated basis functions $\{q_1,q_2,\dots,q_M\}$ that span X_M. Assume also that we have chosen positions $x_1,\dots,x_M$ to locate the first M sensors. The generalized interpolant is assumed to be well defined by (2.4) for $n=M$, i.e.,

$$\mathcal{J}_M[f](\mu)\coloneqq\sum_{j=1}^{M}c_j(\mu)q_j.$$

The coefficients $c_j(\mu),\ j\in\{1,\dots,M\}$, are given by the interpolation problem (2.5) for $n=M$, i.e.,

$$\begin{cases}\text{Find } \{c_j(\mu)\}_{j=1}^M \text{ such that:}\\ \sum\limits_{j=1}^{M}c_j(\mu)B_{k,j}=\sigma\left(f(\cdot,\mu),x_k\right),\ \forall k\in\{1,\dots,M\}.\end{cases}$$

where $B_{k,j}$ are the coefficients of the $M \times M$ matrix $B := \big(\sigma(q_j, x_k)\big)_{1\leq k,j\leq M}$. We now define $f(\cdot, \mu_{M+1})$ such that

$$\|(\phi_i - \mathcal{J}_M[f])(\mu_{M+1})\| = \max_{\mu\in\mathcal{D}} \|(f - \mathcal{J}_M[f])(\mu)\| \tag{2.9}$$

and x_{M+1} such that

$$|\sigma\left((f - \mathcal{J}_M[f])\,(\mu_{M+1}), x_{M+1}\right)| = \max_{x\in\mathcal{R}} |\sigma\left((f - \mathcal{J}_M[f])\,(\mu_{M+1}), x\right)| \tag{2.10}$$

The next basis function is then

$$q_{M+1} = \frac{(f - \mathcal{J}_M[f])(\mu_{M+1})}{\sigma\left((f - \mathcal{J}_M[f])(\mu_{M+1}), x_{M+1}\right)}$$

We finally set $X_{M+1} = \text{span}\{f(\cdot, \mu_j)\}_{j=1}^{M+1} = \text{span}\{q_j\}_{j=1}^{M+1}$ and the generalized interpolant of dimension $M + 1$ of $f(\cdot, \mu)$ is defined in X_{M+1} following formula (2.4) with $n = M + 1$. It satisfies the interpolating conditions (2.5) for the sensors located at the $M + 1$ positions given by the algorithm.

It has been proven in [7] that for any $n \geq 1$, the set $\{q_1, \ldots, q_n\}$ is linearly independent and that this interpolation procedure is well-posed in $\mathcal{X}$. This follows from the fact that the matrix B is lower triangular with diagonal entries equal to 1.

Let us now make several remarks.

i) First of all, note that $\mathcal{D}$ is a set containing parameters in a continuous range so, in practice, it is not possible to compute maximum values over $\mathcal{D}$ as required in formulas (2.6) and (2.9). The same applies for the computation of the maximum over $x \in \mathcal{R}$ in (2.7) and (2.10). This is the reason why it is necessary to consider discrete grids $\mathcal{D}^{(\text{training})}$, $\mathcal{R}^{(\text{training})}$ of $\mathcal{D}$ and $\mathcal{R}$. They have to be fine enough so that the maximum over $\mathcal{D}^{(\text{training})}$ (resp. $\mathcal{R}^{(\text{training})}$) is representative of the maximum over $\mathcal{D}$ (resp. $\mathcal{R}$).

ii) Finally, in practice, problem (2.1) is solved with a numerical scheme that we denote by SOLVE and which yields an approximation $\bar{f}(\cdot, \mu)$ of $f(\cdot, \mu)$,

$$\bar{f}(\cdot, \mu) = \text{SOLVE}\left(\mathcal{F}\left(f, \mu\right) = 0\right).$$

For a given $\mu \in \mathcal{D}^{(\text{training})}$, note that $f(\cdot, \mu)$ is the *exact* solution of the PDE (2.1). So $f(\cdot, \mu)$ is not known exactly but only via an approximation $\bar{f}(\cdot, \mu)$ coming from $\text{SOLVE}\left(\mathcal{F}\left(f, \mu\right) = 0\right)$. $\bar{f}(\cdot, \mu)$ is the quantity that is considered in the practical implementation of the algorithm. For any $\bar{\mu} \in \mathcal{D}^{(\text{training})}$, $\bar{f}(\cdot, \mu)$ is called a snapshot and

$$\mathcal{M}_{\mathcal{D}^{(\text{training})}} \coloneqq \{\bar{f}(\cdot, \mu) \ : \ \mu \in \mathcal{D}^{(\text{training})}\}$$

is called the set of snapshots. It is intended to be representative enough of the set $\mathcal{M}_f$ defined in (2.2). We refer to lemma 1 in [7] for a theoretical discussion on this issue. Another relevant reference is [10] where the authors propose an approach to refine $\mathcal{D}^{(\text{training})}$ by adapting the local approximation spaces to the local anisotropic behavior in the parameter space, thus to be representative enough of the set $\mathcal{M}_f$.

The discretizations ($\mathcal{D}^{(\text{training})}$, $\mathcal{R}^{(\text{training})}$, $\bar{f}$) yield an implementable version of the greedy algorithm which is usually called "weak greedy algorithm". We refer to [7] for a discussion on this point and just give a sketch its practical implementation in algorithm 1. It suffices to remove all the bars in algorithm 1 to fall back to the pure greedy algorithm.

Algorithm 1 Weak Greedy Algorithm

1: $\mu_1 = \arg\max_{\mu \in \mathcal{D}^{(\text{training})}} \|\bar{f}(\cdot, \mu)\|$
2: $x_1 = \arg\max_{x \in \mathcal{R}^{(\text{training})}} |\sigma(\bar{f}(\cdot, \mu_1), x)|$
3: $q_1 = \bar{f}(\cdot, \mu_1)/\sigma(\bar{f}(\cdot, \mu_1), x_1)$
4: **for** n = 2:M **do**
5: $\quad \mu_n = \arg\max_{\mu \in \mathcal{D}^{(\text{training})}} \|(\bar{f} - \mathcal{J}_{n-1}[\bar{f}])(\mu)\|$
6: $\quad x_n = \arg\max_{x \in \mathcal{R}^{(\text{training})}} |\sigma\left((\bar{f} - \mathcal{J}_{n-1}[\bar{f}])(\mu_n), x\right)|$
7: $\quad q_n = (\bar{f} - \mathcal{J}_{n-1}[\bar{f}])(\mu_n)/\sigma\left((\bar{f} - \mathcal{J}_{n-1}[\bar{f}])(\mu_n), x_n\right)$

3. Application to a nuclear reactor core

3.1. Physical model and remarks on how to apply GEIM

In this work, the physical model to describe the flux is the so called transport/diffusion equation. Thus, for a given $\mu \in \mathcal{D}$, the transport/diffusion equation reads

$$\mathcal{A}\left(\phi(\mu), \mu\right) = 0 \tag{3.1}$$

and models how the flux behaves for conditions μ. Since we focus on the neutron flux (and power), the exact solution of (3.1) gives $\phi(\mu)$. For the physical problem that we consider in this paper, the model is the two group neutron diffusion equation. So the flux ϕ has two energy groups $\phi = (\phi_1, \phi_2)$. Index 1 denotes the high energy group and 2 the thermal energy one. The set of parameters is

$$\mu = \{D_1, D_2, \Sigma_{a,1}, \Sigma_{a,2}, \Sigma_{s,1\to2}, \nu\Sigma_{f,1}, \nu\Sigma_{f,2}, \chi_1, \chi_2\}, \tag{3.2}$$

where

- D_i is the diffusion coefficient of group i with $i \in \{1, 2\}$.
- $\Sigma_{a,i}$ is the macroscopic absorption cross section of group i.
- $\Sigma_{s,1\to2}$ is the macroscopic scattering cross section from group 1 to 2.
- $\Sigma_{f,i}$ is the macroscopic fission cross section of group i.
- ν is the average number of neutrons emitted per fission.
- χ_i is the fission spectrum of group i.

For a given μ, the PDE model reads

$$\begin{cases} -\nabla\left(D_1\nabla\phi_1\right) + (\Sigma_{a,1} + \Sigma_{s,1\to 2})\phi_1 = \frac{1}{k_{\text{eff}}}\left(\chi_1\nu\Sigma_{f,1}\phi_1 + \chi_1\nu\Sigma_{f,2}\phi_2\right) \\ -\nabla\left(D_2\nabla\phi_2\right) + \Sigma_{a,2}\phi_2 - \Sigma_{s,1\to 2}\phi_1 = \frac{1}{k_{\text{eff}}}\left(\chi_2\nu\Sigma_{f,1}\phi_1 + \chi_2\nu\Sigma_{f,2}\phi_2\right), \quad \forall x \in \mathcal{R}, \end{cases} \tag{3.3}$$

and the power

$$P = \nu\Sigma_{f,1}\phi_1 + \nu\Sigma_{f,2}\phi_2, \tag{3.4}$$

where k_{eff} is the so-called multiplication factor. We omit here the technical details on the meaning of k_{eff} and refer to general references like [11] or [12, Chapter XXI]. Also, for simplicity in the exposition, we assume in the following that $\phi_1(\mu), \phi_2(\mu), P$ are continuous functions in $\overline{\mathcal{R}}$ (weaker types of regularity could be considered, see [7]). In the numerical computations of section 4, the numerical scheme SOLVE involves the well-known power method to compute k_{eff} and the spacial approximation uses P1 finite elements of a grid of size h (this value will be specified later in section 4). The parameters will be constant or piecewise constant in space but we omit writing explicitly the spacial dependence in order not to overload notation.

If the parameters of our diffusion model range in, say,

$$D_1 \in [D_{1,\min}, D_{1,\max}],\ D_2 \in [D_{2,\min}, D_{2,\max}], \ldots, \chi_2 \in [\chi_{2,\min}, \chi_{2,\max}],$$

then

$$\mathcal{D} \coloneqq [D_{1,\min}, D_{1,\max}] \times \cdots \times [\chi_{2,\min}, \chi_{2,\max}] \tag{3.5}$$

and the set of all possible states of the flux and power is given by

$$\mathcal{M}_{\phi_1,\phi_2,P} \coloneqq \{(\phi_1, \phi_2, P)(\mu)\ :\ \mu \in \mathcal{D}\}, \tag{3.6}$$

which is the manifold of solutions of our problem. Since it is composed of vectorial quantities $(\phi_1, \phi_2, P)(\mu)$, running GEIM in this case is not as straightforward as in the previous section. The reason is that there are plenty of different choices to choose the interpolation points: should one select the x_j with respect to $\phi_1,\ \phi_2,\ P$ or a combination of them? If we choose to work with, say, ϕ_2, how to reconstruct ϕ_1 and P? A first option is to circumvent this issue by viewing the problem differently and defining three independent manifolds

$$\begin{cases} \mathcal{M}_{\phi_1} \coloneqq \{\phi_1(\mu)\ :\ \mu \in \mathcal{D}\} \\ \mathcal{M}_{\phi_2} \coloneqq \{\phi_2(\mu)\ :\ \mu \in \mathcal{D}\} \\ \mathcal{M}_{P} \coloneqq \{P(\mu)\ :\ \mu \in \mathcal{D}\} \end{cases} \tag{3.7}$$

for which we run three separate GEIM algorithms. To go this way, we need to have access to sensor measurements of both ϕ_1 and ϕ_2 and power P. This is in practice not the case since in general it is only possible to measure the thermal flux ϕ_2. For this reason, it is preferable to consider the manifold (3.6) and devise a reconstruction strategy where only thermal flux measurements are taken. We will follow the approach of [2] where the authors reconstruct the velocity and pressure of a fluid by using pressure measurements only. We describe how to adapt the strategy to the current neutronics problem in the next section where we also take into account that there are usually restrictions on the locations to place the sensors in the reactor $\mathcal{R}$. A typical situation is that they can only be placed in the subdomain of $\mathcal{R}$ corresponding to the core $\mathcal{R}_{\text{core}}$ but there are no sensors in the reflector $\mathcal{R}_{\text{refl}}$.

3.2. A GEIM algorithm for the neutronics problem

In the following $\mathcal{C}$ denotes a subdomain of the reactor $\mathcal{R}$ and we assume that $\mathcal{R} = \mathcal{R}_{\text{core}} \cup \mathcal{R}_{\text{refl}}$ and $\mathcal{R}_{\text{core}} \cap \mathcal{R}_{\text{refl}} = \emptyset$. To work with the manifold (3.6), we modify algorithm 1 to approximate the flux and power of $\mathcal{M}_{\phi_1,\phi_2,P}$ when:

- we only use thermal flux measurements (related to ϕ_2)
- the sensors can only be placed in a partial region $\mathcal{C}$ of the reactor, e.g., $\mathcal{C} = \mathcal{R}_{\text{core}}$ or $\mathcal{C} = \mathcal{R}$.

The approach requires that:

- the Kolmogorov n-width of $\mathcal{M}_{\phi_1,\phi_2,P}$ decays fast
- the thermal flux sensors' satisfy the *unisolvence property*
- the mapping $\phi_2(\mu) : \mathcal{D} \to \mathcal{M}_{\phi_1,P}$ is one to one (we comment on this hypothesis at the end of the section)

We start by defining μ_1 as the quantity maximizing

$$\max \left(\max_{\mu\in\mathcal{D}} \|\phi_1(\mu)\|,\ \max_{\mu\in\mathcal{D}} \|\phi_2(\mu)\|,\ \max_{\mu\in\mathcal{D}} \|P(\mu)\| \right). \tag{3.8}$$

This yields $X_1^1 = \text{span}\{\phi_1(\mu_1)\}$, $X_1^2 = \text{span}\{\phi_2(\mu_1)\}$ and $X_1^P = \text{span}\{P(\mu_1)\}$. The first sensor location x_1 is now the one such that

$$|\sigma(\phi_2, x_1)| = \max_{x\in\mathcal{C}} |\sigma(\phi_2, x)|. \tag{3.9}$$

For any $\mu \in \mathcal{D}$, we can then define $\mathcal{J}_1[\phi_2](\mu)$ as in the previous algorithm (see 3.10), i.e.

$$\mathcal{J}_1[\phi_2](\mu) \coloneqq c_1^{(2)}(\mu) q_1^{(2)}. \tag{3.10}$$

Expressing $\mathcal{J}_1[\phi_2](\mu)$ with the snapshot $\phi_2(\mu_1)$, we equivalently have

$$\mathcal{J}_1[\phi_2](\mu) \coloneqq d_1(\mu)\phi_2(\mu_1). \tag{3.11}$$

Since we no longer have at hand either $\sigma(\phi_1, x_1)$ nor $\sigma(P, x_1)$, we cannot reconstruct ϕ_1 and P as before. One option is to use the coefficient $d_1(\mu)$ to approximate ϕ_1 and P with

$$\widetilde{\mathcal{J}}_1[\phi_1](\mu) = d_1(\mu)\phi_1(\mu_1) \tag{3.12}$$

and

$$\widetilde{\mathcal{J}}_1[P](\mu) = d_1(\mu)P(\mu_1). \tag{3.13}$$

Then we define

$$J_1[\phi_1, \phi_2, P](\mu) = d_1(\mu) \begin{bmatrix} \phi_1(\mu_1) \\ \phi_2(\mu_1) \\ P(\mu_1) \end{bmatrix} \tag{3.14}$$

as the interpolant of $(\phi_1(\mu), \phi_2(\mu), P(\mu))$.

For subsequent dimensions, we proceed by induction. We assume that, for a given $M > 1$, we have selected $\{\mu_1, \ldots, \mu_M\}$ and we have the set of locations $\{x_1, \ldots, x_M\}$ for the sensors of ϕ_2. We also assume that the generalized interpolant for ϕ_2,

$$\mathcal{J}_M[\phi_2](\mu) \coloneqq \sum_{j=1}^{M} d_j(\mu)\phi_2(\mu_j),$$

is well defined. The approximation of $(\phi_1(\mu), \phi_2(\mu), P(\mu))$ reads

$$J_M[\phi_1, \phi_2, P](\mu) = \sum_{j=1}^{M} d_j \begin{bmatrix} \phi_1(\mu_j) \\ \phi_2(\mu_j) \\ P(\mu_j) \end{bmatrix}. \tag{3.15}$$

We then define μ_{M+1} as the parameter which maximizes

$$\max \begin{pmatrix} \max_{\mu\in\mathcal{D}} \frac{\|(\phi_1 - J_M[\phi_1,\phi_2,P]_{\phi_1})(\mu)\|}{\|\phi_1(\mu)\|} \\ \max_{\mu\in\mathcal{D}} \frac{\|(\phi_2 - J_M[\phi_1,\phi_2,P]_{\phi_2})(\mu)\|}{\|\phi_2(\mu)\|} \\ \max_{\mu\in\mathcal{D}} \frac{\|(P - J_M[\phi_1,\phi_2,P]_{P})(\mu)\|}{\|P(\mu)\|} \end{pmatrix}, \tag{3.16}$$

where we use relative errors in order to deal with possible differences in the magnitude orders of ϕ_1, ϕ_2 and P. Finally, the next sensor location x_{M+1} satisfies

$$|\sigma\left((\phi_2 - \mathcal{J}_M[\phi_2])(\mu_{M+1}), x_{M+1}\right)| = \max_{x\in\mathcal{C}} |\sigma\left((\phi_2 - \mathcal{J}_M[\phi_2])(\mu), x\right)| \tag{3.17}$$

and the inductive step is completed.

Contrary to $\mathcal{J}_n[\phi_2](\mu)$, note that $J_M[\phi_1, \phi_2, P]_{\phi_1}$ and $J_M[\phi_1, \phi_2, P]_P$ are not interpolants of ϕ_1 and P since they do not satisfy any interpolation condition of the type (2.5). The tilde in the notation is there to stress on this fact. However, as we will see in section 4, the approach yields a good accuracy in the numerical simulations that we have considered. We again emphasize that the same approach was used in [2] in a Stokes problem with a good accuracy in the reconstruction. The reference might be of interest to the community studying thermal-hydraulics in reactor cores.

Before giving some numerical results, a remark on the hypothesis that the mapping $\phi_2(\mu) : \mathcal{D} \to \mathcal{M}_{\phi_1,P}$ is one to one is in order. It is quite obvious that for $f = \phi_1$, ϕ_2 and P the mapping $f(\cdot, \mu) : \mathcal{D} \to \mathcal{M}_f$ is *one to one* and this allows to reconstruct the fluxes and power based on measurements of each of these. Similarly, the mapping $(\phi_1, \phi_2, P)(\mu) : \mathcal{D} \to \mathcal{M}_{\phi_1,\phi_2,P}$ is one to one. However, there is an obstruction to reconstruct $(\phi_1, \phi_2, P)(\mu)$ from measurements only acquired from thermal flux $\phi_2(\mu)$ without assuming that $\phi_2(\mu) : \mathcal{D} \to \mathcal{M}_{\phi_1,P}$ is one to one. Indeed, if it were not one to one, for a given μ there could be several states for ϕ_1 (resp. P) in $\mathcal{M}_{\phi_1}$ (resp. $\mathcal{M}_P$) and the quality of approximation with only ϕ_2 measurements is no longer ensured.

4. Numerical examples: search for sensor locations for flux and power reconstruction

In this section, we apply the methodology described in section in section 3.2 to two simple examples in which ϕ_1, ϕ_2 and P are reconstructed with the only knowledge of thermal flux measurements. We consider two cases:

- Case I: the sensors can be placed at any point, in section 3.2, the partial region $\mathcal{C} = \mathcal{R}$.
- Case II: the admissible sensor locations are restricted to the core $\mathcal{R}_{\text{core}}$, which corresponds to setting $\mathcal{C} = \mathcal{R}_{\text{core}}$ in the algorithm of section 3.2.

With these two cases, we aim to show how the algorithm can be adapted to explore different restrictions in the positioning of the sensors.

4.1. A classical 1D example

We consider the classical 1D test case presented in [13, Chapter 4]. The reactor domain is $\mathcal{R} = [0, 30\text{cm}]$. The core and the reflector are $\mathcal{R}_{\text{core}} = [0, 25\text{cm}]$ and $\mathcal{R}_{\text{refl}} = [25, 30\text{cm}]$ respectively. We consider only the value of $D_1|_{\mathcal{R}_{\text{refl}}}$ in the reflector $\mathcal{R}_{\text{refl}}$ as a parameter (so $p = 1$ and $\mu = D_1|_{\mathcal{R}_{\text{refl}}}$). We assume that $D_1|_{\mathcal{R}_{\text{refl}}} \in [0.5, 2.0]$. The rest of the coefficients of the diffusion model (3.3) (including $D_1|_{\mathcal{R}_{\text{core}}}$) are fixed to the values indicated on table 4.1. In principle, one could also consider these coefficients as parameters but we have decided to focus only on $D_1|_{\mathcal{R}_{\text{refl}}}$ because of its crucial role in the physical estate of the core: its variation can be understood as a change in the boundary conditions in $\mathcal{R}_{\text{core}}$ which, up to a certain extent, allows to compensate the bias of the diffusion model with respect to reality.

	Core		Reflector	
Energy group	1	2	1	2
χ	1.0	0.0	0.0	0.0
$\nu\Sigma_f(\text{cm}^{-1})$	0.0085	0.1851	0.0	0.0
$\Sigma_a(\text{cm}^{-1})$	0.0121	0.121	0.0004	0.020
$\Sigma_s^{1\to2}(\text{cm}^{-1})$	0.0241	–	0.0493	–
$D(\text{cm})$	1.267	0.354	$\in$ [0.5,2.0]	0.166

Table 4.1: Coefficient values.

In figure 1 we show some examples of the behavior of (ϕ_1, ϕ_2, P) for different values of the parameter $D_1|_{\mathcal{R}_{\text{refl}}}$. For any $D_1|_{\mathcal{R}_{\text{refl}}} \in [0.5, 2.0]$, we propose to reconstruct (ϕ_1, ϕ_2, P) as outlined at the end of section 2, i.e., we approximate ϕ_2 with its generalized interpolant $\mathcal{J}_n[\phi_2]$ (see (3.10)). ϕ_1 and P will be reconstructed with $J_M[\phi_1, \phi_2, P]_{\phi_1}$ and $J_M[\phi_1, \phi_2, P]_P$ as defined in (3.12) and (3.13). Note that in this simple case we clearly satisfy that $\phi_2(\mu) : \mathcal{D} \to \mathcal{M}_{\phi_1,P}$ is a one to one mapping (one can visually verify it in figure 1).

For this, we run a weak greedy algorithm over a set of 300 snapshots of ϕ_2 (solutions of the PDE for a discrete grid $\mathcal{D}^{(\text{training})} \subset \mathcal{D}$ of 300 parameters). The admissible domain for the search of the interpolating points is either $\mathcal{C} = \mathcal{R}$ (case I) or $\mathcal{C} = \mathcal{R}_{\text{core}}$ (case II).

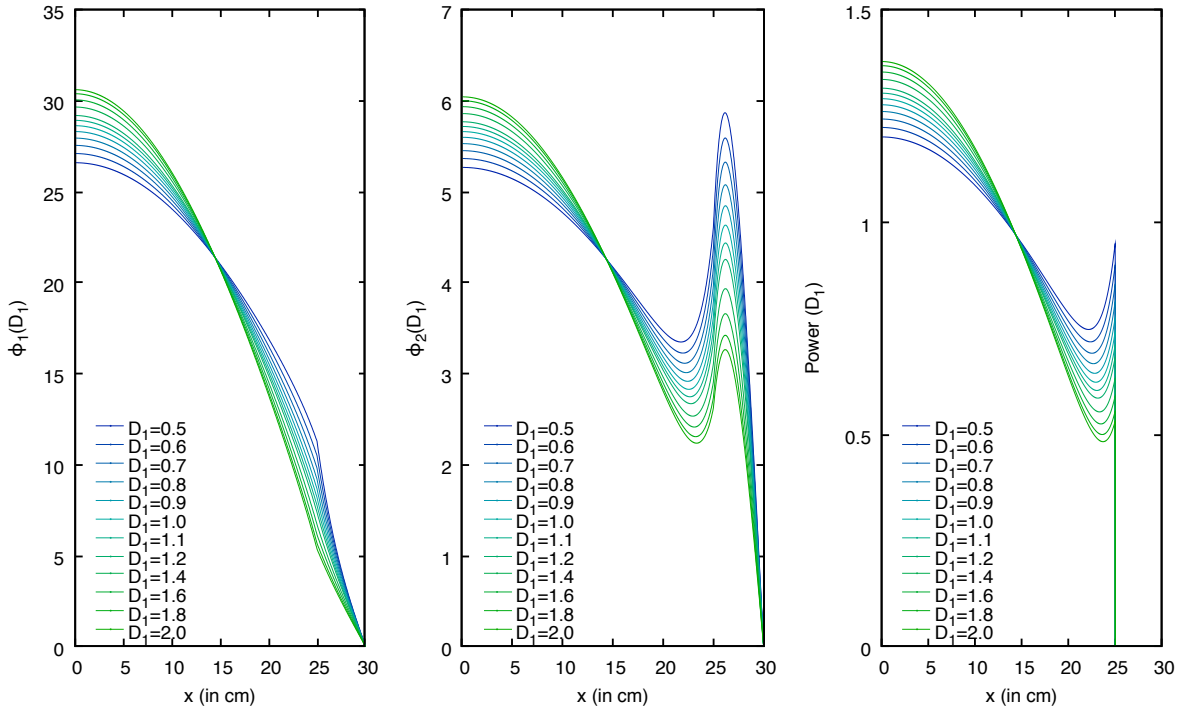

Figure 1: (ϕ_1, ϕ_2, P) for different values of $D_1|_{\mathcal{R}_{\text{refl}}}$. The values have been normalized to a reference quantity.

Let us now turn to the analysis of the results. Figure 2 shows the sensor locations given by the greedy algorithm in cases I and II. We study the performance of the reconstruction strategy by considering first of all the decay of the errors

$$e_n^{(\text{training})}(\phi_2) := \max_{\mu \in \mathcal{D}^{(\text{training})}} \|\phi_1(\mu) - \mathcal{J}_n[\phi_2](\mu)\|_{L^2(\mathcal{R})} \tag{4.1}$$

in the greedy algorithm. Here we present plots of case I and case II, need to recognize that both case I and case II yield very similar results, we only analysis plots of case II for the sake of concision. In figure 4a, the decay is compared to an indicator of the optimal performance in $L^2(\mathcal{R})$ which is obtained by a singular value decomposition of the snapshots $\phi_2(\mu),\ \forall \mu \in \mathcal{D}^{(\text{training})}$. Note that $e_n^{(\text{training})}(\phi_2)$ decays at a similar rate as the SVD which suggests that GEIM behaves in a quasi-optimal way (see [7]). We now estimate the accuracy to reconstruct $(\phi_1, \phi_2, P)(D_1|_{\mathcal{R}_{\text{refl}}})$ for any $D_1|_{\mathcal{R}_{\text{refl}}} \in [0.5, 2.0]$ which does not necessary belong to the training set of snapshots. For this, we consider a test set of 300 parameters $\mathcal{D}^{(\text{test})}$ different from $\mathcal{D}^{(\text{training})}$ and compute the errors

$$\begin{cases} e_n^{(\text{test})}(\phi_1) & := \max_{\mu \in \mathcal{D}^{(\text{test})}} \|\phi_1(\mu) - J_M[\phi_1, \phi_2, P]_{\phi_1}(\mu)\|_{L^2(\mathcal{R})} \\ e_n^{(\text{test})}(\phi_2) & := \max_{\mu \in \mathcal{D}^{(\text{test})}} \|\phi_1(\mu) - J_M[\phi_1, \phi_2, P]_{\phi_2}(\mu)\|_{L^2(\mathcal{R})} \\ e_n^{(\text{test})}(P) & := \max_{\mu \in \mathcal{D}^{(\text{test})}} \|P(\mu) - J_M[\phi_1, \phi_2, P]_{P}(\mu)\|_{L^2(\mathcal{R})} \end{cases} \tag{4.2}$$

The decay of the errors (4.2) is plotted in figure 4b. The fact that $e_n^{(\text{test})}(\phi_2)$ decays very similarly to $e_n^{(\text{training})}(\phi_2)$ confirms that the set of 300 training snapshots was representative enough of the whole manifold. Also, the fast decay of $e_n^{(\text{test})}(\phi_1)$ and $e_n^{(\text{test})}(P)$ shows that the use of the operator $\widetilde{\mathcal{J}}_n$ to approximate ϕ_1 and P is accurate enough[2].

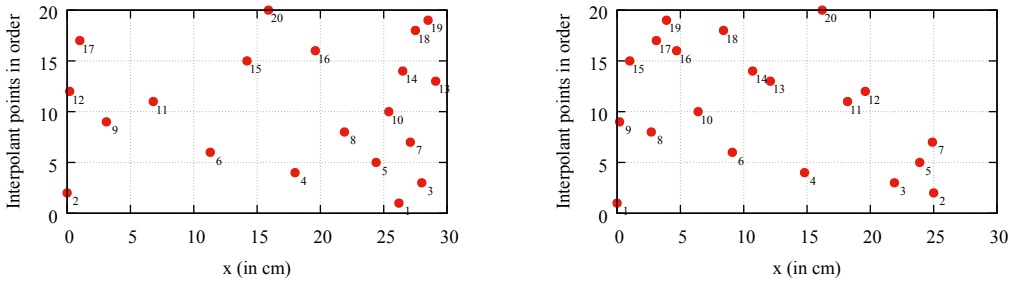

(a) Case I (selection in $\mathcal{R}$) (b) Case II (selection in $\mathcal{R}_{\text{core}}$)

Figure 2: Locations of the sensors chosen by the greedy algorithm.

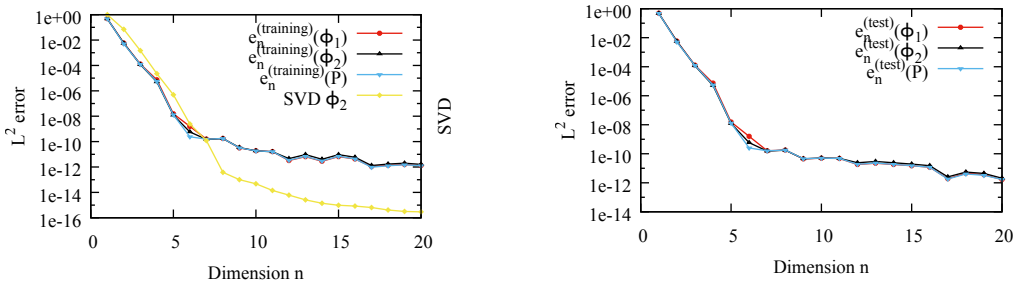

(a) Decay of SVD modes and of $e_n^{(\text{training})}(\phi_1, \phi_2, P)$.

(b) Decay of $e_n^{(\text{test})}(\phi_1)$, $e_n^{(\text{test})}(\phi_2)$ and $e_n^{(\text{test})}(P)$.

Figure 3: Case I, $L^2(\mathcal{R})$ norm: Reconstruction of $(\phi_1, \phi_2, P)(\mu)$ with $J_M[\phi_1, \phi_2, P](\mu)$.

[2]In this work, the snapshots are generated by solving (3.3) with the power method in which the spacial discretization involves P1 finite elements on a grid of size $h = 0.01$ cm. It follows that the accuracy of the snapshots is of order $\mathcal{O}(h)$ in $L^2(\mathcal{R})$ and, since the greedy algorithm of GEIM is based upon these snapshots, the best accuracy that one can retrieve in the reconstruction will also be $\mathcal{O}(h)$. Because of this accuracy limits, we note that in Figure 3 - Figure 8, the information from dimension 6 to dimension 20 is of no meaning .

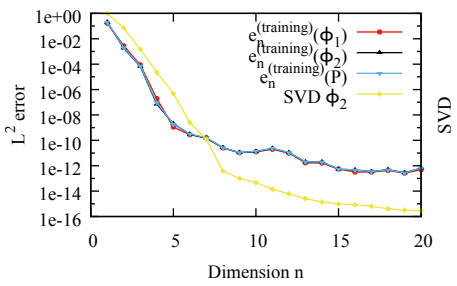

(a) Decay of SVD modes and of $e_n^{(\text{training})}(\phi_1, \phi_2, P)$.

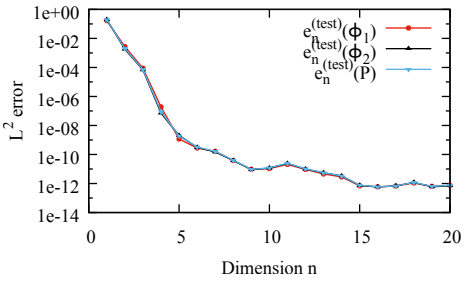

(b) Decay of $e_n^{(\text{test})}(\phi_1)$, $e_n^{(\text{test})}(\phi_2)$ and $e_n^{(\text{test})}(P)$.

Figure 4: Case II, $L^2(\mathcal{R})$ norm: Reconstruction of $(\phi_1, \phi_2, P)(\mu)$ with $J_M[\phi_1, \phi_2, P](\mu)$.

Instead of working with $L^2(\mathcal{R})$, it is also possible to work with other norms (provided some spacial regularity in the manifold). A particularly relevant case in neutronics is $L^\infty(\mathcal{R})$. Figure 6 shows the results of the reconstruction procedure when working in this norm and figure 8 shows the behavior when considering the $H^1(\mathcal{R})$ and working with the semi-norm $|u|_{H^1(\mathcal{R})} = \int_{\mathcal{R}} |\nabla u|^2$ (energy norm).

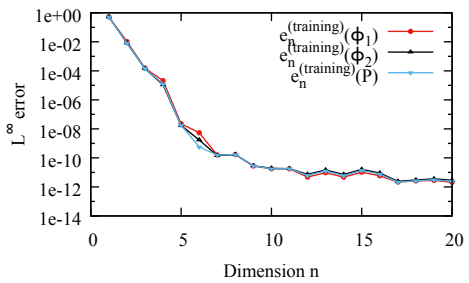

(a) Decay of the greedy errors $e_n^{(\text{training})}(\phi_1, \phi_2, P)$.

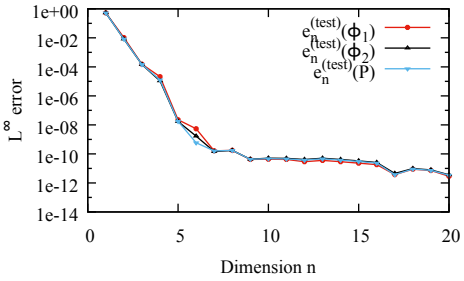

(b) Decay of $e_n^{(\text{test})}(\phi_1)$, $e_n^{(\text{test})}(\phi_2)$ and $e_n^{(\text{test})}(P)$.

Figure 5: Case I, $L^\infty(\mathcal{R})$ norm: Reconstruction of $(\phi_1, \phi_2, P)(\mu)$ with $J_M[\phi_1, \phi_2, P](\mu)$.

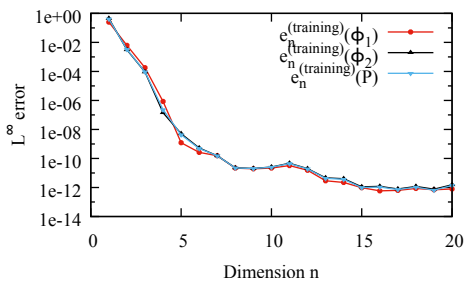

(a) Decay of the greedy errors $e_n^{(\text{training})}(\phi_1, \phi_2, P)$.

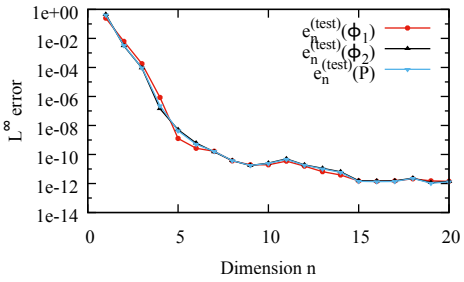

(b) Decay of $e_n^{(\text{test})}(\phi_1)$, $e_n^{(\text{test})}(\phi_2)$ and $e_n^{(\text{test})}(P)$.

Figure 6: Case II, $L^\infty(\mathcal{R})$ norm: Reconstruction of $(\phi_1, \phi_2, P)(\mu)$ with $J_M[\phi_1, \phi_2, P](\mu)$.

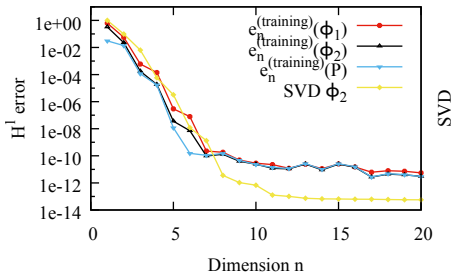

(a) Decay of SVD modes and of $e_n^{(\text{training})}(\phi_1, \phi_2, P)$.

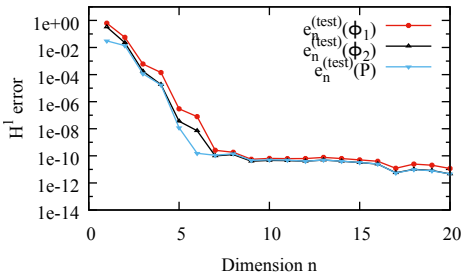

(b) Decay of $e_n^{(\text{test})}(\phi_1)$, $e_n^{(\text{test})}(\phi_2)$ and $e_n^{(\text{test})}(P)$.

Figure 7: Case I, $H^1(\mathcal{R})$ norm: Reconstruction of $(\phi_1, \phi_2, P)(\mu)$ with $J_M[\phi_1, \phi_2, P](\mu)$.

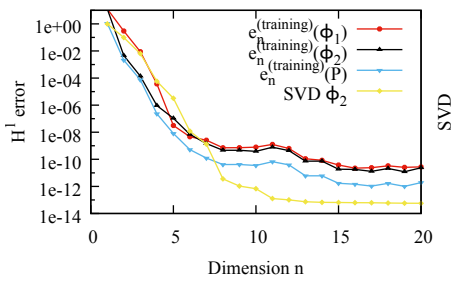

(a) Decay of SVD modes and of $e_n^{(\text{training})}(\phi_1, \phi_2, P)$.

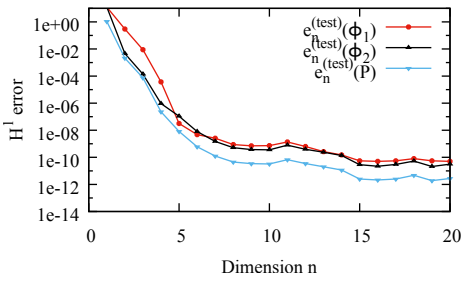

(b) Decay of $e_n^{(\text{test})}(\phi_1)$, $e_n^{(\text{test})}(\phi_2)$ and $e_n^{(\text{test})}(P)$.

Figure 8: Case II, $H^1(\mathcal{R})$ norm: Reconstruction of $(\phi_1, \phi_2, P)(\mu)$ with $J_M[\phi_1, \phi_2, P](\mu)$.

4.2. A 2D example

We then consider the classical 2D IAEA Benchmark Problem [**?**], the core geometry which can be seen in figure 9. The problem conditions and the requested results are stated

in page 437 of reference [**?**]. It is identified with the code 11-A2, and its descriptive title is Two-dimensional LWR Problem, also known as 2D IAEA Benchmark Problem. This problem represents the mid-plane $z = 190\ cm$ of the 3D IAEA Benchmark Problem, that is used by references [**?**] and show in application within [**?**].

Figure 9 shows the sensor locations given by the greedy algorithm in cases I and II. In the same spirit as the example in 1D, figures 11, 13 and 15 present the errors in $L^2(\mathcal{R})$, $L^\infty(\mathcal{R})$ and $H^1(\mathcal{R})$ of the greedy algorithm phase and over the test set $\mathcal{D}^{(\text{test})}$. Similarly as in 1D, the convergence of the algorithm decays exponentially and illustrates the potential of the method to reconstruct flux and power with a few sensors.

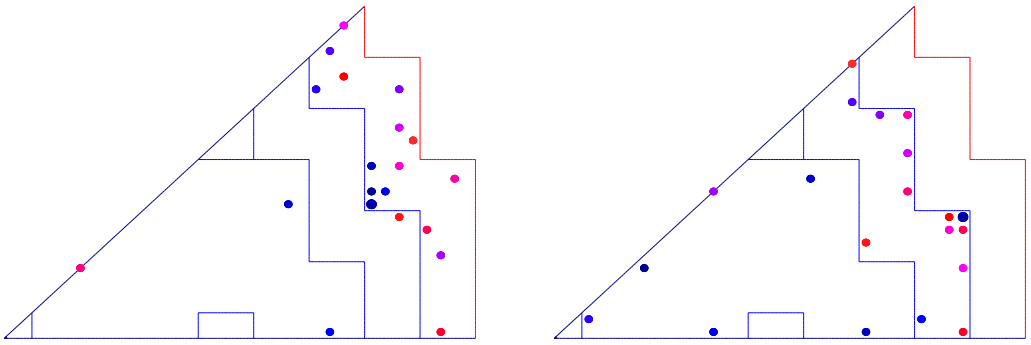

(a) Case I (selection in $\mathcal{R}$) (b) Case II (selection in $\mathcal{R}_{\text{core}}$)

Figure 9: Locations of the sensors chosen by the greedy algorithm.

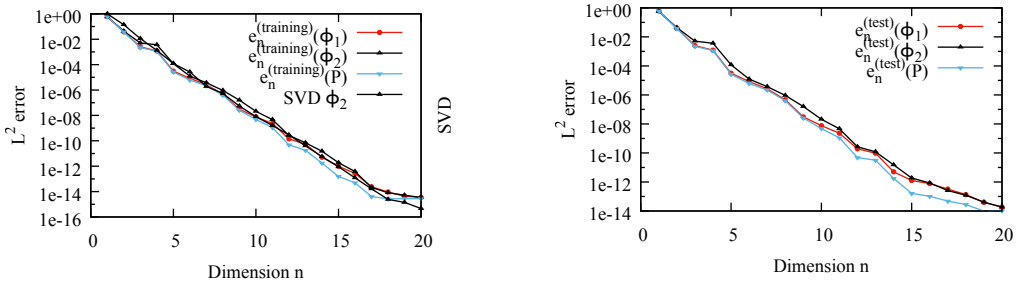

(a) Decay of SVD modes and of $e_n^{(\text{training})}(\phi_1, \phi_2, P)$.

(b) Decay of $e_n^{(\text{test})}(\phi_1)$, $e_n^{(\text{test})}(\phi_2)$ and $e_n^{(\text{test})}(P)$.

Figure 10: Case I, $L^2(\mathcal{R})$ norm: Reconstruction of $(\phi_1, \phi_2, P)(\mu)$ with $J_M[\phi_1, \phi_2, P](\mu)$.

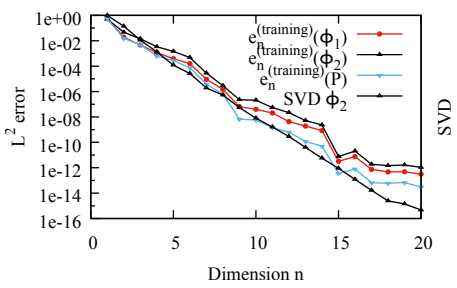

(a) Decay of SVD modes and of $e_n^{(\text{training})}(\phi_1, \phi_2, P)$.

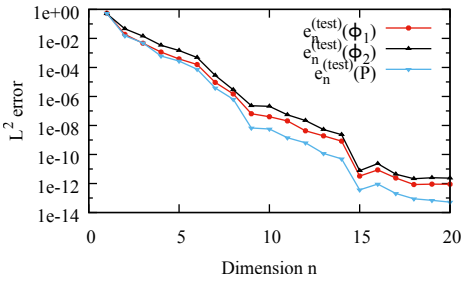

(b) Decay of $e_n^{(\text{test})}(\phi_1)$, $e_n^{(\text{test})}(\phi_2)$ and $e_n^{(\text{test})}(P)$.

Figure 11: Case II, $L^2(\mathcal{R})$ norm: Reconstruction of $(\phi_1, \phi_2, P)(\mu)$ with $J_M[\phi_1, \phi_2, P](\mu)$.

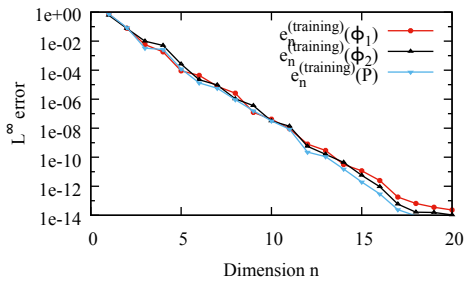

(a) Decay of the greedy errors $e_n^{(\text{training})}(\phi_1, \phi_2, P)$.

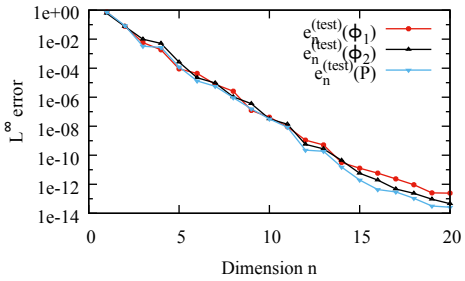

(b) Decay of $e_n^{(\text{test})}(\phi_1)$, $e_n^{(\text{test})}(\phi_2)$ and $e_n^{(\text{test})}(P)$.

Figure 12: Case I, $L^\infty(\mathcal{R})$ norm: Reconstruction of $(\phi_1, \phi_2, P)(\mu)$ with $J_M[\phi_1, \phi_2, P](\mu)$.

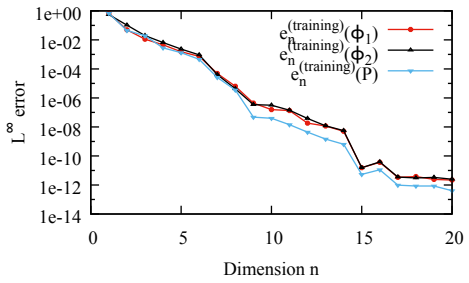

(a) Decay of the greedy errors $e_n^{(\text{training})}(\phi_1, \phi_2, P)$.

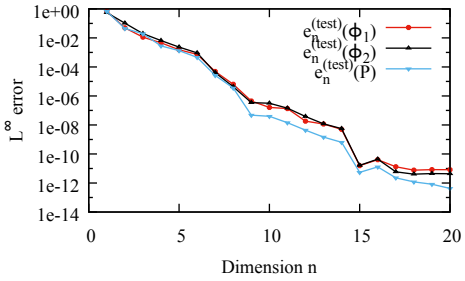

(b) Decay of $e_n^{(\text{test})}(\phi_1)$, $e_n^{(\text{test})}(\phi_2)$ and $e_n^{(\text{test})}(P)$.

Figure 13: Case II, $L^\infty(\mathcal{R})$ norm: Reconstruction of $(\phi_1, \phi_2, P)(\mu)$ with $J_M[\phi_1, \phi_2, P](\mu)$.

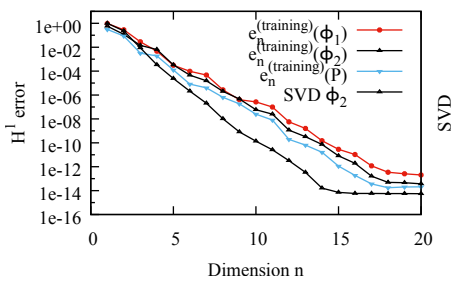

(a) Decay of SVD modes and of $e_n^{(\text{training})}(\phi_1, \phi_2, P)$.

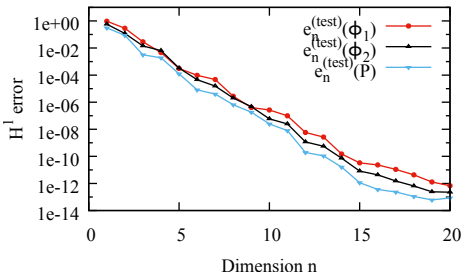

(b) Decay of $e_n^{(\text{test})}(\phi_1)$, $e_n^{(\text{test})}(\phi_2)$ and $e_n^{(\text{test})}(P)$.

Figure 14: Case I, $H^1(\mathcal{R})$ norm: Reconstruction of $(\phi_1, \phi_2, P)(\mu)$ with $J_M[\phi_1, \phi_2, P](\mu)$.

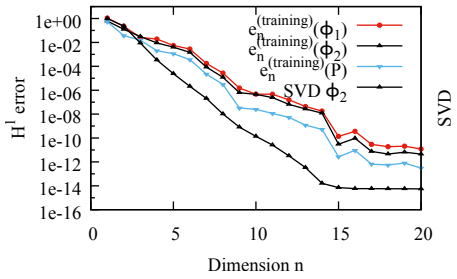

(a) Decay of SVD modes and of $e_n^{(\text{training})}(\phi_1, \phi_2, P)$.

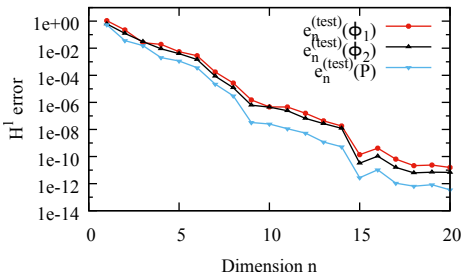

(b) Decay of $e_n^{(\text{test})}(\phi_1)$, $e_n^{(\text{test})}(\phi_2)$ and $e_n^{(\text{test})}(P)$.

Figure 15: Case II, $H^1(\mathcal{R})$ norm: Reconstruction of $(\phi_1, \phi_2, P)(\mu)$ with $J_M[\phi_1, \phi_2, P](\mu)$.

5. More general methods beyond GEIM and future works

As already brought up in the introduction, GEIM belongs to a broader class of methods which couple reduced models with measured data. In particular, the so-called PBDW (Parametrized Backgroup Data Weak, [3]) is an extension in which it is possible to work with a number m of sensors which is not necessarily equal to the reduced basis space X_n. In fact, it is required that $m \geq n$ since PBDW involves a least squares method instead of an interpolation in order to approximate the functions. The fact that $m \geq n$ is also the key to be capable of taking the model bias into account (see [3, 5]). In future works, we will present results with more focus on this aspect. We will also extend the results of [14, 15] on how to adapt the methodology to take into account noise in the measurements. In parallel to these developments, more theoretical works on the stability of the method are also ongoing.

[1] Y. Maday and O. Mula. A Generalized Empirical Interpolation Method: application of reduced basis techniques to data assimilation. In Franco Brezzi, Piero Colli Franzone, Ugo Gianazza, and Gianni Gilardi, editors, *Analysis and Numerics of Partial Differential Equations*, volume 4 of *Springer INdAM Series*, pages 221–235. Springer Milan, 2013.

[2] Y. Maday, O. Mula, A. T. Patera, and M. Yano. The Generalized Empirical Interpolation Method: stability theory on Hilbert spaces with an application to the Stokes equation. *Computer Methods in Applied Mechanics and Engineering*, 287(0):310–334, 2015.

[3] Y. Maday, A. T. Patera, J. D. Penn, and M. Yano. A Parameterized-Background Data-Weak approach to variational data assimilation: formulation, analysis, and application to acoustics. *International Journal for Numerical Methods in Engineering*, 102(5):933–965, 2015.

[4] B. Peherstorfer and K. Willcox. Dynamic data-driven reduced-order models. *Computer Methods in Applied Mechanics and Engineering*, 291:21–41, 2015.

[5] P. Binev, A. Cohen, W. Dahmen, R. DeVore, G. Petrova, and P. Wojtaszczyk. Data assimilation in reduced modeling. *SIAM/ASA Journal on Uncertainty Quantification*, 5(1):1–29, 2017.

[6] R. DeVore, G. Petrova, and P. Wojtaszczyk. Data assimilation in Banach spaces. *arXiv preprint arXiv:1602.06342*, 2016.

[7] Y. Maday, O. Mula, and G. Turinici. Convergence analysis of the generalized empirical interpolation method. *SIAM Journal on Numerical Analysis*, 54(3):1713–1731, 2016.

[8] H. Gong, J.P. Argaud, B. Bouriquet, and Y. Maday. The Empirical Interpolation Method applied to the neutron diffusion equations with parameter dependence. In *Proceedings of Physor*, 2016.

[9] A. Cohen and R. DeVore. Kolmogorov widths under holomorphic mappings. *IMA Journal of Numerical Analysis*, page dru066, 2015.

[10] Yvon Maday and Benjamin Stamm. Locally adaptive greedy approximations for anisotropic parameter reduced basis spaces. *SIAM Journal on Scientific Computing*, 35(6):A2417–A2441, 2013.

[11] A. Hebert. *Applied reactor physics*. Presses inter Polytechnique, 2009.

[12] R. Dautray and J.-L. Lions. *Mathematical Analysis and Numerical Methods for Science and Technology: Volume 6 Evolution Problems II*. Springer Science & Business Media, 2012.

[13] Weston M Stacey. *Nuclear reactor physics*. John Wiley & Sons, 2001.

[14] Y. Maday, A. T. Patera, J. D. Penn, and M. Yano. PBDW State Estimation: Noisy Observations; Configuration-Adaptive Background Spaces, Physical Interpretations. *ESAIM: Proceedings and Surveys*, 50:144–168, 2015.

[15] J.P. Argaud, B. Bouriquet, H. Gong, Y. Maday, and O. Mula. Stabilization of (g)eim in presence of measurement noise: application to nuclear reactor physics. 2016. https://arxiv.org/pdf/1611.02219.pdf.